Nano Research
2021, 14(11): 4243–4249
ISSN 1998-0124 CN 11-5974/O4
https://doi.org/10.1007/s12274-021-3596-4

Research Article

Enhanced efficiency of top-emission InP-based green quantum dot light-emitting diodes with optimized angular distribution

Dong Li, Jingwen Feng, Youqin Zhu, Zhigao Lu, Chen Pei, Zhuo Chen (✉), Yanzhao Li (✉), Xinguo Li (✉), and Xiaoguang Xu (✉)

BOE Technology Group Co., Ltd., Beijing 100176, China

Received: 23 March 2021 / **Revised:** 16 May 2021 / **Accepted:** 17 May 2021

ABSTRACT

High resolution and wide color gamut are two key requirements for novel display technologies. Owing to the distinguishing advantages over conventional displays, such as intrinsic wide color gamut and the possibility to achieve high resolution, quantum dot light-emitting diodes (QLED) have drawn considerable attention in recent years. On the other hand, indium phosphide quantum dots (InP QDs) have shown a great potential as a replacement for cadmium selenide (CdSe) QDs in display applications due to the inherent toxicity of cadmium-based QDs. In this study, we investigate a top-emission InP-based green QLED with optimized angular distribution. By adjusting the electrical and optical architecture, the device exhibits improved properties with a maximum current efficiency of 30.1 cd/A and a narrowed full width at half maxima (FWHM)of 31 nm, which are the best results ever reported to our knowledge.

KEYWORDS

Cd-free quantum dots, quantum dot light-emitting diode (QLED), top-emission, angular distribution, current efficiency

1 Introduction

In the modern information society, consumers pay more attention to the user experience of display products, including the image quality, power consumption, smart system, fashion and environmental friendly. The key requirements for novel display technologies focus on high resolution and wide color gamut (WCG). Organic light-emitting diodes (OLEDs) [1–3], micro-LEDs [4, 5], quantum dot light-emitting diodes (QLEDs) [6–9], laser display [10] and several other emerging technologies [11–13] have been vigorously developed to meet these market trends. Among them, QLEDs have earned much attention as the next generation display technology owing to the distinguishing advantages over others, such as intrinsic WCG and the possibility to achieve high resolution [14].

Colloidal quantum dots (QDs) show unique optical and electrical properties, which are determined by their particle size, resulting into electronic structure fundamentally different from bulk semiconductor materials due to the quantum confinement effect. Since the first report of QDs in 1994 [15], rapid progress has been made by many research groups to enhance performance of light-emitting devices via both material and device structure optimization [16–18]. However, most of the reported QLED devices are fabricated with heavy metal, such as cadmium (Cd), which is known to be highly toxic to the environment. In recent years, the use of these hazardous materials has become a big concern, and has been strictly limited by regulations such as Restriction of Hazardous Substances (RoHS), making it critical to search for alternative Cd-free materials. Thus, Cd-free QDs are attracting interests, among which indium phosphide (InP) QDs are considered as the most promising candidate because of their well-matched energy levels and considerable photoluminescence quantum yield (PLQY) [19–21]. By controlling the confinement of electron and hole wave functions under the electric field and the charge balance in the devices, high PLQY of InP-based QDs and improved performance of the InP-based QLEDs can be accomplished. In order to promote QLED technologies rapidly into products, it demands the joint efforts of academia and industry to develop the QLEDs structures with remarkable performances and nontoxicity QDs, which are suitable for the industrial production. As the head display manufacturers, Samsung, LG, BOE and TCL etc. have invested plenty of R&D works which mostly focus on the nontoxicity QLEDs together with high resolution.

Over the past several years, many researches have focused on the improvement of InP-based QLEDs [22–30]. The current efficiency of red InP-based QLED has broken through 20 cd/A which is catching up with Cd-based QLED [24]. The research works in green InP-based QLEDs which are infrequently reported compared to red InP-based QLEDs. Lim et al. reported InP-based green QLEDs using (poly[(9,9-bis(30-(N,N-dimethylamino)propyl)-2,7-fluorene)-alt-2,7-(9,9-ioctylfluorene) (PFN) as an interlayer between the electron transport layer (ETL) and the emissive layer (EML) and a thick ZnSeS heterostructured shell to enhance the electron–hole balance and to reduce the Auger recombination process [26]. Zhang et al. also reported green QLEDs using InP/GaP/ZnS QDs with a

Address correspondence to Zhuo Chen, chenzhuo_cto@boe.com.cn; Yanzhao Li, liyanzhao@boe.com.cn; Xinguo Li, lixinguo@boe.com.cn; Xiaoguang Xu, xuxiaoguang@boe.com.cn

thick shell which can reduce nonradiative Föster resonant energy transfer between QDs [27]. Chae et al. reported that utilizing composition-tailored ZnMgO nanoparticles as ETL can reduce the electron mobility of the ETL and improve the band alignment between ETL and the InP-based QDs [28]. In 2020, our group has reported the highest current efficiency of 37 cd/A for green InP-based QLED [29]. However, all the devices exhibited broad full width at half maxima (FWHM) of over 40 nm, due to the limitation of the InP QDs materials.

Among the above works, the most widely used device structure was bottom-emission, in which light emits through the glass substrate. Because the light cannot go through the driving circuits of the back plane when using the bottom-emission structure, the aperture ratio will be limited to an extremely low level, which limits the panel resolution. However, high resolution is one of the most important market trends for display products, including mobile phones and 8K TVs. In order to obtain high aperture ratio, the top-emission structure, in which light emits through the top transparent or semitransparent electrodes and thus vests the freedom of pixel and circuit design, is becoming increasingly important. In addition, by controlling the microcavity length between two metal electrodes via tuning the transport layer thickness in top-emission QLEDs, a much lower waveguide loss of light extraction and stronger vertical emission can be obtained [30, 31]. As a result, we can get higher current efficiency and narrower FWHM in top-emission device. However, there are only few reports about the top-emission QLEDs. In 2019, Kwak group reported a top-emission InP-based QLED by introducing a hole-suppressing interlayer, obtaining a current efficiency of 21.6 and 8.5 cd/A, FWHM of 37 and 38 nm for green and red devices, respectively [30]. They are the most promising results for top-emission InP-based QLEDs reported thus far.

In this study, we fabricated green top-emission InP-based QLED devices with optimized angular distribution. By optimizing the electrical and optical architecture, the device exhibited improved properties with a maximum current efficiency of 30.1 cd/A and a narrowed FWHM of 31 nm. To the best of our knowledge, they are the best results among the recent reports on green top-emission InP-based QLEDs. The simulated angle distribution of these devices was also in good agreement with measured results, which could do great favor to the device architecture design.

2 Results and discussion

An organic-inorganic hybrid device architecture was adopted for InP-based QLEDs, and the schematic structure and energy diagram were illustrated in Fig. 1. In the bottom–emission devices, a transparent ITO was utilized as the bottom electrode, while a reflective Ag/ITO bottom electrode was employed in top-emitting devices.

The device structures were Glass/ITO/ZnMgO or ZnO/InP GQD/TCTA/NPB/HAT-CN/Ag, and Glass/Ag/ITO/ZnMgO or ZnO/InP GQD/TCTA/NPB/HAT-CN/Ag for bottom- and top-emission devices, respectively. 2,3,6,7,10,11-Hexaaza-triphenylenehexacabonitrile (HAT-CN) was used as the hole injection layer (HIL). 4,4',4"-tris(carbazol-9-yl)-triphenylamine (TCTA) and N,N'-diphenyl-N,N'-bis(1-naphthyl)-1,1'-biphenyl-4,4"-diamine (NPB) were adopted as a double layer hole transport layer (HTL), because the HOMO level of TCTA is close to the HOMO level of InP-based green QDs (InP GQDs). Green-emitting InP/ZnSe/ZnS core/shell-structured QDs were used as an EML. The QDs have a PLQY of 60%, a PL peak wavelength at 533 nm, and the spectral FWHM of 41 nm under solution conditions. ZnO or ZnMgO was utilized as the ETL. The Ag thickness were 150 and 15 nm in bottom-emission and top-emission devices, respectively. All the devices were fabricated and encapsulated according to the description in section "Device fabrication". The electrons and holes are injected from the ITO cathode and Ag anode, respectively, and then recombined at the QDs layer to achieve luminescence [16]. The energy band structure of the QLED devices is shown in Fig. 1(b).

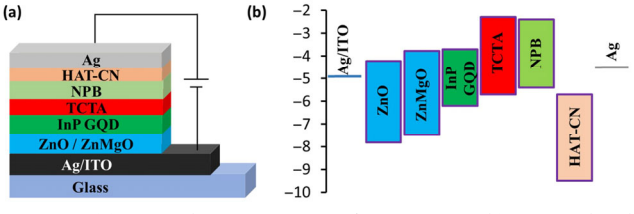

Figure 1 (a) Basic device structure of InP QLED. (b) Energy band diagrams of InP QLEDs with ZnO, ZnMgO ETLs.

The PLQY of emitters play an important role in the efficiency of electroluminescent devices. It has been reported previously that PLQY of InP-based QDs can be very high in solution environment, but decreases significantly after depositing into a film [32]. It has also been shown that when more than one layers are deposited consequentially, a donor-acceptor relationship can be formed between them [33]. To find the effect of the ZnO and/or ZnMgO underlayer on photoluminescence properties of InP GQDs, PLQY measurements had been performed on the samples consisting of a ZnMgO or ZnO ETL film and an InP GQD film formed consequentially on a glass substrate. It was shown in Fig. 2(a) that when undoped ZnO ETL was used as underlayer, PLQY of G-InP QD droped form 49.2% to 48.6%, which was a very slight decrease. With the Mg doping, the efficiency reduction was more severe, resulting into 44.1% PLQY.

It has been reported that the process of QD quenching by ZnO/ZnMgO nanoparticles has two components: one is electron transfer from InP QDs to ZnO/ZnMgO nanoparticles (dynamic quenching); and the other is related to the decrease of emitting centers in InP QDs, possibly through tethering of QDs to the surface of ZnO/ZnMgO nanoparticles (static quenching) [22, 34].

A further support for the quenching mechanism was provided by time-resolved photoluminescence (TRPL) measurements as shown in Figs. 2(b) and 2(c). The average exciton decay times (τ_{avg}) of InP GQD films were 49.9, 50.0, and 41.3 ns for the InP QD films on glass, ZnO, and ZnMgO underlayers, respectively. It suggests that the quenching by ZnO films is slighter than ZnMgO film, which can fully account for substantial changes in PLQY seen in Fig. 2(a).

Another important factor to affect device performance is the charge balance between electrons and holes in QDs [17, 35]. Hole current and electron current within QLED devices were then investigated to evaluate the charge balance between electrons and holes injected into QDs for the following device performance improvement. To verify the electron injection and transport capabilities of ZnO and ZnMgO films, and compare them with the hole injection and transport capabilities of HIL/HTL, the electron-only (EOD) and hole-only devices (HOD) were fabricated. The fabrication conditions for EODs and HODs are identical to the full device fabrication conditions and are explained in the Device Fabrication section of the paper. Device structures were as follows: ITO/ZnO/InP GQD/ZnO/Ag (ZnO EOD), ITO/ZnMgO/InP GQD/ZnMgO/Ag (ZnMgO EOD), and ITO/TFB/InP GQD/TCTA/NPB/HAT-CN/Ag (HOD). Here, the poly(9,9-dioctylfluorene-alt-N-(4-sec-butylphenyl)-diphenylamine) (TFB) is used as the electron

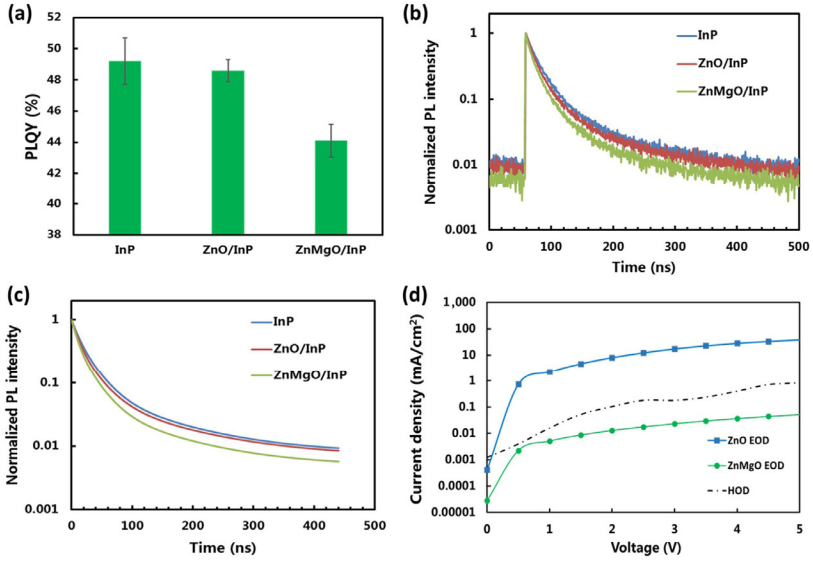

Figure 2 (a) PLQY of green InP QD films on different underlayers (Glass, Glass/ZnO, and Glass/ZnMgO). (b) The raw data of TRPL decay curves of the films of green InP QD films on different underlayers (Glass, Glass/ZnO, and Glass/ZnMgO). (c) The double exponential fitted curves of the raw data. (d) Current density vs. voltage characteristics of EOD and HOD devices.

blocking layer, because it won't be affected by the solution process of the following QD films. On the other hand, TFB is an HTL material and the hole mobility of TFB is several orders much higher than the mobility of the TCTA and NPB, allowing to detect a net hole current density exclusively dependent on the HIL and HTL of the devices, respectively. In our opinion, the device structures we chose for EODs and HODs can provide a reasonable enough approximation of electrons and holes dynamics in real devices. Thus, the injection and transport capabilities can be adequately enough characterized by measuring current density–voltage (*J*–*V*) characteristics of these devices, as shown in Fig. 2(d). It is evident that the electron current density of ZnO EOD is much higher than the hole current density of HOD, because of the higher mobility of ZnO than organic HTL materials. And with Mg doping, the electron density of ZnMgO EOD decreases a lot due to the higher resistance of ZnMgO than ZnO [22, 36], and becomes significantly lower than the hole current density of HOD. It means that the charge balance behaviors between the devices using ZnMgO and ZnO ETL differ a lot, and different optimization directions need to be taken to obtain better charge balance.

The ZnO ETL was firstly used in our bottom-emission QLED devices to investigate the electrical properties. To adjust the charge balance, we varied different HTL/HIL, and ETL thickness, and compared the device performances, separately. The current density–voltage–luminance *(J–V–L)* characteristics and current efficiency of these QLEDs with different thickness were shown in Fig. 3. As shown in Fig. 3(a), the current density and luminance increased while the HTL thickness decreased, which is contributed to the improved hole injection. Considering the excess electron injection in the QLEDs with ZnO ETL, decreasing the HTL thickness can help with the charge balance, which improved the current efficiency (Fig. 3(b)). On the other hand, we can see from Fig. 3(c) that the luminance did not change a lot with the ZnO ETL thickness increased, while the current density decreased a lot. Thus, the current efficiency had an obvious increase with the ZnO thickness (Fig. 3(d)). A maximum current efficiency of 16.8 cd/A was achieved when 70 nm ZnO and 5 nm/30 nm TCTA/NPB was utilized.

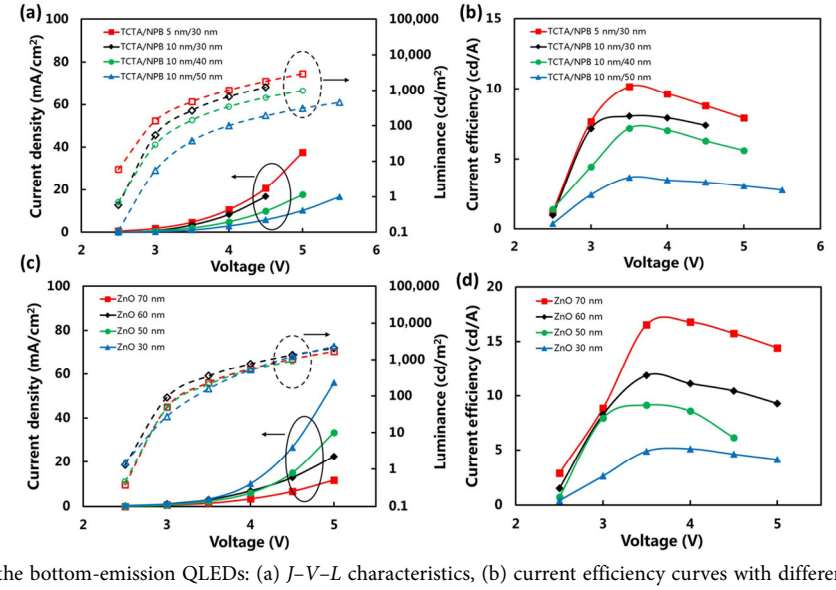

Figure 3 Performance of the bottom-emission QLEDs: (a) *J*–*V*–*L* characteristics, (b) current efficiency curves with different HTL thickness; (c) *J*–*V*–*L* characteristics, (d) current efficiency curves with different ZnO ETL thickness.

After the electrical optimization in bottom-emission devices, the light extraction behaviors of the top-emission devices with different HTL/ETL thickness were investigated. We can consider this top-emission structure as a Fabry-Perot cavity, in which the emitter is situated between a bottom reflective mirror formed by Ag/ITO cathode (bottom contact) and a top semitransparent mirror formed by a thin Ag anode (top contact). In such a cavity, two types of interferences can be found: (1) interference between directly emitted light and the light reflected from the bottom mirror with the same wave vector (wide-angle interference) and (2) interference between the light multiply reflected from bottom and top mirrors (multiple-beam interference) [22, 37].

In the cavity model, the emitted irradiance can be expressed as [31]:

$$I(\lambda,\theta)=\frac{T_t\left[1+R_b+2\sqrt{R_b}\cos\left(-f_b+\frac{4\pi n(\lambda)d'\cos(\theta'_{EML})}{\lambda}\right)\right]}{(1-\sqrt{R_bR_t})^2+4\sqrt{R_bR_t}\sin^2\left(\frac{\Delta\phi}{2}\right)}I_0(\lambda) \quad (1)$$

where λ is the emission wavelength, θ is the emitting angle in the air, T_t is the transmittance through the top contact, R_t is the reflectivity of the top contact, R_b is the reflectivity of the bottom contact, θ'_{EML} is the corresponding light propagation angle in the organic layer governed by the Snell's law, ϕ_b is the phase shift of the bottom contact, $n(\lambda)$ is the refractive index of the material in dependence of the wavelength, $\Delta\phi$ is the phase shift after one cycle, $I_0(\lambda)$ is the intrinsic PL spectra intensity of the radiating molecules, and d' is their distance to the highly reflecting mirror.

Further, the phase shift of the light wave after one cycle in the cavity is given by [31, 37]:

$$\Delta\phi=-\phi_b+\sum_i\frac{4\pi n'_i(\lambda)d'_i\cos(\theta'_i)}{\lambda} \quad (2)$$

or

$$\Delta\phi=-\phi_b-\phi_t+\sum_i\frac{4\pi n_i(\lambda)d_i\cos(\theta'_i)}{\lambda} \quad (3)$$

where ϕ_b is the phase shift of the bottom contact, ϕ_t is the phase shift of the top contact, $n'_i(\lambda)$ and d'_i are the refractive index and thicknesses of the layers from the radiating molecules to the highly reflecting mirror, $n_i(\lambda)$ and d_i are the refractive index and thicknesses of all the layers within the cavity. Equations (2) and (3) stand for the wide-angle interference and multiple-beam interference, respectively.

The resonance conditions should be determined when $\Delta\phi = 2\pi m$ (m = 0,1,2…). If the resonant conditions are reached, constructive interference is achieved, resulting into enhanced emission. It can be easily seen from the equations that the resonant conditions are dependent on the emitting wavelength of the emitter, optical length of the cavity, position of the emitter within the cavity relative to the reflective and semitransparent mirrors, and also the emitting angle. If resonant conditions are not reached, the interference stops being constructive, and the emission from the microcavity is suppressed.

From the equations above, we can also calculate the irradiance intensity in dependence of the emitting angle, $I(\theta)$, by Eq. (4) once the intrinsic PL spectra intensity $I_0(\lambda)$, optical length of the cavity and the distance from the emitter to the reflective bottom electrode are given.

$$I(\theta)=\sum_i I(\lambda_i,\theta) \quad (4)$$

We performed optical simulations using SETFOS semiconducting thin-film optics simulation software to determine optimal layer thicknesses for achieving stronger vertical emission in the top-emitting green QLED devices (Fig. 4(a)). Here, a semi-transparent 15 nm-thick Ag was used as the top electrode. It can be clearly seen that top-emitting devices have a strong optical cavity, because the good vertical emission can be only achieved in a very small range of HTL/ETL thickness (from 20 to 40 nm for both HTL and ETL). The simulated angular distribution of the EL emission with different ZnO ETL and HTL is plotted in Figs. 4(b) and 4(c). We can see that for both ETL and HTL, the thickness should be in the range from 20 to 40 nm in order to achieve stronger vertical emission. It means that the light extraction to the normal direction is increased due to the enhanced out-coupling in these structures. For this reason, the current efficiency of the top-emission QLEDs should be superior to that of the bottom-emission QLEDs using suitable HTL/ETL thickness, even though the top-emission QLEDs exhibit similar external quantum efficiency (EQE) with the bottom-emission QLEDs, or even slightly lower EQE. However, an obvious contradiction appear in the devices using ZnO ETL, when combining the electrical and optical simulation results together. For HTL thickness, we need about 30 nm to get better electrical results, which is located in the range of optical simulation results. But for ZnO ETL thickness, we need

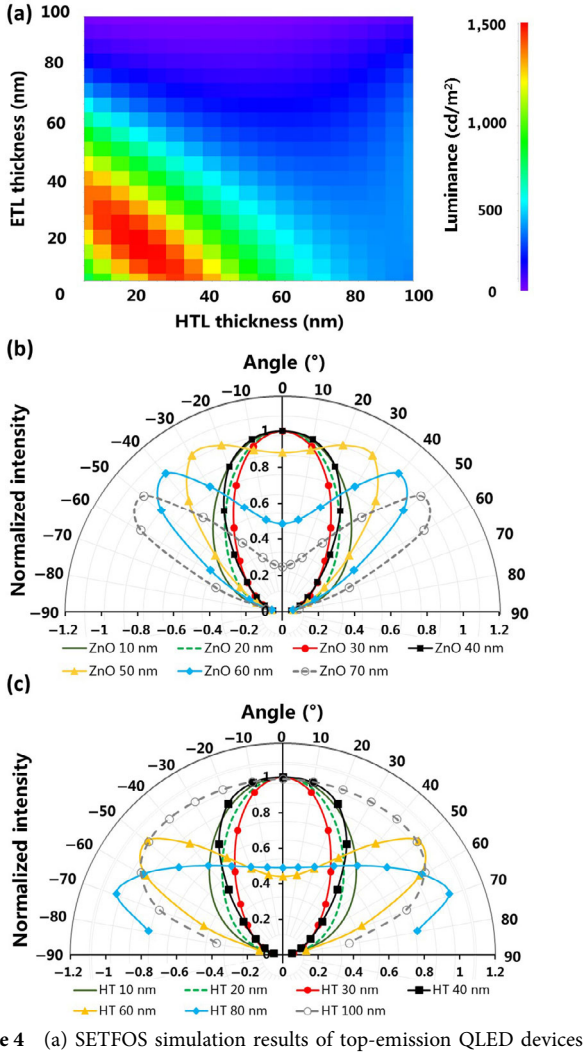

Figure 4 (a) SETFOS simulation results of top-emission QLED devices luminance dependence on HTL and ETL thickness. The simulated normalized angle-dependent EL intensity of the top-emission QLEDs with different (b) ZnO ETL (the HTL thickness is 30 nm) and (c) HTL thickness (the ETL thickness is 30 nm).

about 70 nm to get better electrical results, which is out of the range of optical simulation results.

The top-emission QLED devices performances with 30 nm HTL and different ZnO ETL thickness were then investigated. The *J*–*V*–*L* characteristics and current efficiency of these QLEDs with changing thickness were shown in Fig. 5.

With the ZnO thickness from 30 to 70 nm, the device luminance decreased significantly. In comparison with Fig. 3, the maximum current efficiency of bottom-emission devices were 5.1, 9.1, 11.9 and 16.8 cd/A (1.3%, 2.3%, 3.1% and 4.3% for EQE), with the ZnO thickness of 30, 50, 60, and 70 nm, respectively. While the maximum current efficiency of top-emission devices were 12.0, 8.1, 1.8 and 0.86 cd/A (1.0%, 1.2%, 2.2% and 2.6% for EQE), respectively. These results are in good agreement with the optical simulation results, in which the vertical emission will be much lower with thicker ZnO thickness (i.e., above 60 and 70 nm) than thinner ZnO thickness (i.e., below 40 nm). We also measured the angle distribution of top-emission QLED devices with different ZnO ETL thickness, as shown in Fig. 5(c).

Due to the similar optical parameters between ZnMgO and ZnO, the simulated angular distribution of the ZnMgO devices is nearly the same with ZnO devices. Fortunately, as the electron injection is more difficult than hole injection in ZnMgO devices (as shown in Fig. 2(d)), it is possible for us to make a device with thin ZnMgO ETL to achieve both better charge balance and higher vertical light extraction.

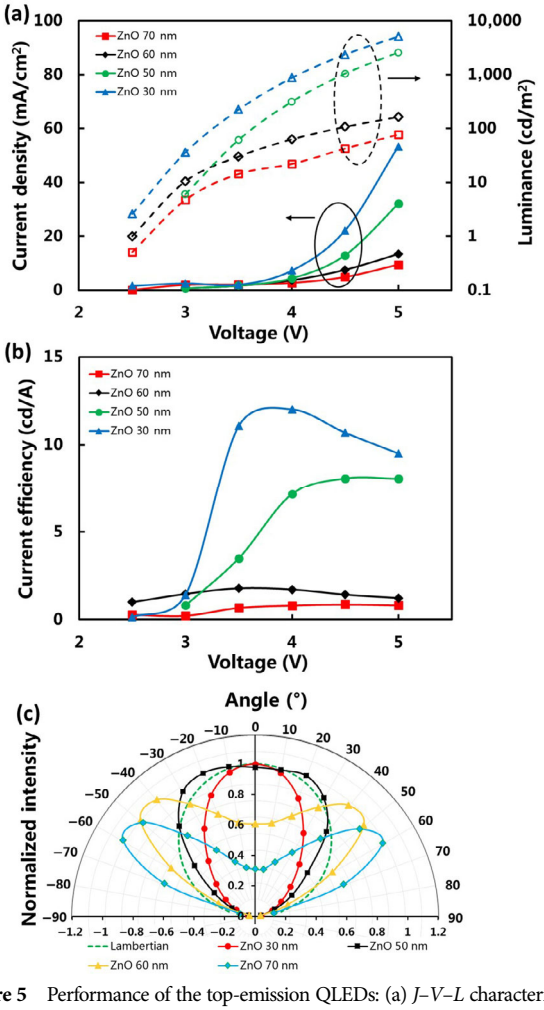

Figure 5 Performance of the top-emission QLEDs: (a) *J*–*V*–*L* characteristics, (b) current efficiency curves with different ZnO ETL thickness. (c) The measured normalized angle-dependent EL intensity of the top-emission QLEDs with different ZnO ETL (the HTL thickness is 30 nm).

The bottom- and top-emission QLED devices performances with 30 nm HTL and different ZnMgO ETL thickness were investigated to support our claim. The *J*–*V*–*L* characteristics and current efficiency of these QLEDs with changing thickness were shown in Fig. 6. Due to the different particle sizes and ligands, the thickness of ZnMgO and ZnO are slightly different under the same solution concentration and rotation speed. In bottom-emission devices, from Fig. 6(a), with the ZnMgO thickness from 80 to 35 nm, both the device current density and luminance increased, following the same trend as the current efficiency as shown in Fig. 6(b), which means better charge balance. However, when the ZnMgO thickness was reduced to 20 nm, the current density sharply increased, with a slight decrease for the luminance. Thus, the current efficiency was much lower than the device with 35 nm ZnMgO. We think it might be due to the too thin ETL which could cause large current leakage or over-injected electron, resulting into the unbalanced charge injection. The maximum current efficiency of bottom-emission devices were 8.2, 22.5, 6.4 and 4.6 cd/A (2.1%, 5.6%, 1.6% and 1.1% for EQE), with the ZnMgO thickness of 20, 35, 60, and 80 nm, respectively. Though the ZnMgO has more severe effect on PL quenching of InP QDs than ZnO as shown in Fig. 2(b), the maximum EQE of ZnMgO devices are slightly higher than the ZnO devices. It may be due to that the ZnMgO devices exhibit more balanced charge injection than the ZnO devices.

In top-emission devices, from Fig. 6(c), the luminance increased with the ZnMgO thickness from 80 to 20 nm, which should be due to the enhanced vertical emission with thinner ZnMgO thickness. The maximum current efficiency of top-emission devices were 12.3, 30.1, 3.8 and 1.5 cd/A (2.0%, 4.2%, 1.4% and 1.2% for EQE), respectively, as shown in Fig. 6(d). As the relatively lower vertical emission with thicker ZnMgO thickness (above 60 nm) than thinner ZnMgO thickness (below 40 nm), we obtained a higher top-emission efficiency than bottom efficiency with the ZnMgO thickness of 20 and 35 nm, and on the contrary, a lower top-emission efficiency with the ZnMgO thickness of 60 and 80 nm.

The angular distribution of top-emission QLED devices with different ZnMgO ETL thickness was also measured and summarized in Fig. 7(a). These results are in good agreement with that the vertical emission was much lower with thicker ZnMgO thickness (i.e., 60 and 80 nm) than thinner ZnMgO thickness (i.e., 20 and 35 nm). Thus the top-emission devices with thiner ZnMgO exhibited higher current efficiency than bottom-emission devices. It means that the electrical and optical optimization results were in good agreement with each other. At last, the comparison of the normalized EL spectra for bottom- and top-emission devices was presented in Fig. 7(b). The measured spectrum of the top-emission devices showed a significant improvement in FWHM compared with the bottom-emission devices—it was reduced from 41 to 31 nm, and the Commission Internationale de Eclairage (CIE) index was improved from (0.240, 0.712) to (0.205, 0.763), which are comparable to the FWHM and chromatic coordinates of CdSe-based G-QLEDs. This result can be also explained by the microcavity formation between a reflective bottom electrode (ITO/Ag) and a semi-reflective top electrode (Ag, 15 nm) of devices with top-emitting architecture. Because only a relatively narrow distribution of the emission spectra can satisfy the resonant conditions, this will result into narrower FWHM. The improved current efficiency and FWHM values suggest that using a top-emission structure is advantageous for the implementation of WCG QLED displays in terms of both optical and electrical properties.

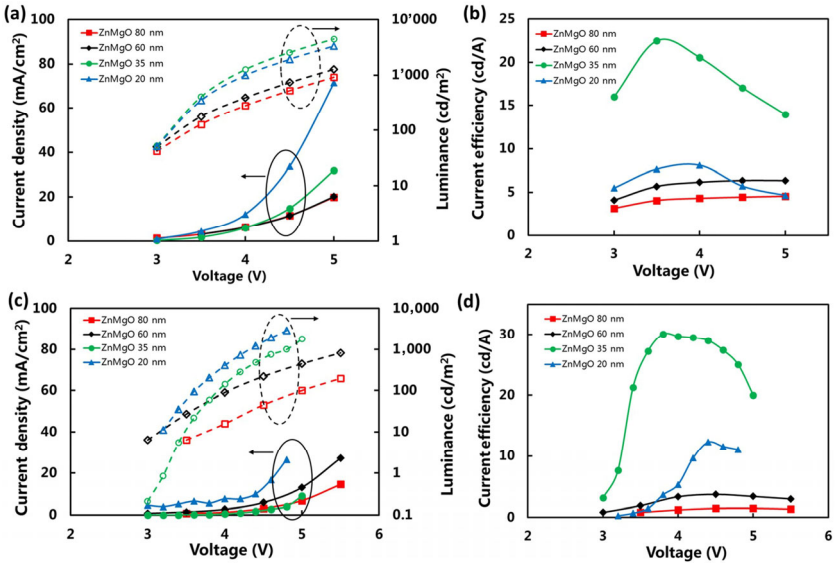

Figure 6 Performance of the bottom- and top-emission QLEDs with different ZnMgO ETL thickness. Bottom-emission QLEDs: (a) *J*–*V*–*L* characteristics, (b) current efficiency curves. Top-emission QLEDs: (c) *J*–*V*–*L* characteristics, (d) current efficiency curves (the HTL thickness is 30 nm).

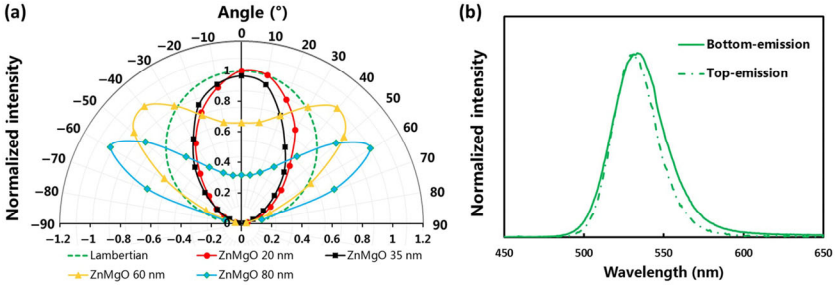

Figure 7 (a) The measured normalized angle-dependent EL intensity of the top-emission QLEDs with different ZnMgO ETL (the HTL thickness is 30 nm). (b) Comparation of the normalized EL spectra between the bottom- and top-emission QLED devices.

3 Conclusions

In summary, we demonstrated high performance top-emission InP-based green QLEDs. Based on the device engineering, our top-emission QLEDs exhibited remarkably higher efficiency and narrowed FWMH than any other InP-based QLEDs. The superb performance is achieved by controlling both the electrical charge balance and optical microcavity. Utilizing ZnMgO as the ETL, we can obtain enhanced vertical light extraction and improved charge balance in the same range of transport layer thickness. A very high current efficiency of 30.1 cd/A and narrow FWMH of 31 nm for InP-based green top-emission QLED devices were achieved in this study, which is the best results ever reported as far as we know. We believe that our research can be capable of providing next generation nontoxic QLED displays with improved efficiency and color purity.

4 Experimental section/methods

4.1 Device fabrication

The green InP-based QDs and ZnMgO nanoparticles were purchased from Mesolight Inc., and ZnO nanoparticles were supplied by Poly OptoElectronics TECH. Ltd. (PolyOE, China). The QLED devices were fabricated through spin-coating and evaporation on glass substrates with pre-patterned ITO (for bottom-emission) and Ag/ITO (for top-emission) electrodes. The substrates were carefully cleaned in deionized water, acetone and ethyl alcohol for 15 min each, and then treated with UV-ozone for another 5 min. Subsequently, an ETL material of ZnO or ZnMgO nanoparticles was spin-coated on the substrate for 40 s, and then annealed at 120 °C for 20 min in a N_2-filled glovebox. Next, green InP QDs nanocrystals was deposited on the substrates under identical conditions (at 2,500 rpm for 40 s if not specified otherwise). Furthermore, the thickness of each layer had been adjusted by changing the solution concentration and spin-coat speed. Green InP QDs were deposited from an octane solution, ZnO and ZnMgO were deposited from ethanol solution. After the deposition of the solution-processed layers, all samples were transferred to a vacuum deposition chamber with chamber pressure below 10^{-6} torr ($P < 10^{-6}$ torr). TCTA, NPB, HAT-CN and Ag with different thickness were deposited consequentially in a vacuum chamber, followed by the encapsulation with a UV-curable epoxy and cover glasses in N_2 atmosphere. The Ag thickness were 150 and 15 nm in bottom-emission and top-emission devices, respectively. The organic materials and Ag thickness were controlled by the quartz crystal oscillator with the deposition rate of 0.5–1 Å/s.

4.2 Device characterization

The *J*–*V*–*L*, and EL spectra characteristics of the QLEDs were measured using a Keithley 2400 multimeter, and a photonic multichannel analyzer (PMA, Hamamatsu). The angle distribution was measured using the PMA, with the samples mounted onto the rotating stage. The PLQYs of QDs were measured by the Hamamatsu C9920 absolute PL quantum yield spectrometer. The transient PL decay curves were measured by the Spectrofluorometer FS5 from Edinburgh instruments. The thicknesses of the spin-coated and evaporated films were measured using the Bruker's DektakXT stylus profiler.

Acknowledgements

This work was supported by the National Key R&D Program of China under Grant No. 2016YFB0401700.

References

[1] Salehi, A.; Fu, X. Y.; Shin, D. H.; So, F. Recent advances in OLED optical design. *Adv. Funct. Mater*. **2019**, *29*, 1808803.

[2] Wei, Q.; Fei, N.; Islam, A.; Lei, T.; Hong, L.; Peng, R. X.; Fan, X.; Chen, L.; Gao, P. Q.; Ge, Z. Y. Small-molecule emitters with high quantum efficiency: Mechanisms, structures, and applications in OLED devices. *Adv. Opt. Mater.* **2018**, *6*, 1800512.

[3] Wu, J. B.; Agrawal, M.; Becerril, H. A.; Bao, Z. N.; Liu, Z. F.; Chen, Y. S.; Peumans, P. Organic light-emitting diodes on solution-processed graphene transparent electrodes. *ACS Nano* **2010**, *4*, 43–48.

[4] Wu, T. Z.; Sher, C. W.; Lin, Y.; Lee, C. F.; Liang, S. J.; Lu, Y. J.; Chen, S. W. H.; Guo, W. J; Kuo, H. C.; Chen, Z. Mini-LED and Micro-LED: Promising candidates for the next generation display technology. *Appl. Sci.* **2018**, *8*, 1557.

[5] Huang, Y. G.; Tan, G. J; Gou, F. W; Li, M. C.; Lee, S. L.; Wu, S. T. Prospects and challenges of mini-LED and micro-LED displays. *J. Soc. Inf. Disp*. **2019**, *27*, 387–401.

[6] Rogach, A. L.; Gaponik, N.; Lupton, J. M.; Bertoni, C.; Gallardo, D. E.; Dunn, S.; Pira, N. L.; Paderi, M.; Repetto, P.; Romanov, S. G. et al. Light-emitting diodes with semiconductor nanocrystals. *Angew. Chem., Int. Ed.* **2008**, *47*, 6538–6549.

[7] Pietryga, J. M.; Park, Y. S.; Lim, J.; Fidler, A. F.; Bae, W. K.; Brovelli, S.; Klimov, V. I. Spectroscopic and device aspects of nanocrystal quantum dots. *Chem. Rev.* **2016**, *116*, 10513–10622.

[8] Liu, Y.; Jiang, C. B.; Song, C.; Wang, J. H.; Mu, L.; He, Z. W.; Zhong, Z. J.; Cun, Y. K.; Mai, C. H.; Wang, J. et al. Highly efficient all-solution processed inverted quantum dots based light emitting diodes. *ACS Nano* **2018**, *12*, 1564–1570.

[9] Shirasaki, Y.; Supran, G. J.; Bawendi, M. G.; Bulovic, V. Emergence of colloidal quantum-dot light-emitting technologies. *Nat. Photonics* **2013**, *7*, 13–23.

[10] Yuan, Y.; Bi, Y.; Sun, M. Y.; Wang, D. Z.; Wang, D. D.; Gao, W. N.; Zhang, S. Speckle evaluation in laser display: From speckle contrast to speckle influence degree. *Opt. Commun*. **2020**, *454*, 124405.

[11] Yaras, F.; Kang, H.; Onural, L. Circular holographic video display system. *Opt. Express* **2011**, *19*, 9147–9156.

[12] Zhang, L. Q.; Yang, X. L.; Jiang, Q.; Wang, P. Y.; Yin, Z. G.; Zhang, X. W; Tan, H. R; Yang, Y. M.; Wei, M. Y.; Sutherland, B. R. et al. Ultra-bright and highly efficient inorganic based perovskite light-emitting diodes. *Nat. Commun.* **2017**, *8*, 15640.

[13] Xiao, Z. G; Kerner, R. A.; Zhao, L. F; Tran, N. L.; Lee, K. M.; Koh, T. W.; Scholes, G. D.; Rand, B. P. Efficient perovskite light-emitting diodes featuring nanometre-sized crystallites. *Nat. Photonics* **2017**, *11*, 108–115.

[14] Mei, W. H; Zhang, Z. Q.; Zhang, A. D.; Li, D.; Zhang, X. Y.; Wang, H. W.; Chen, Z.; Li, Y. Z.; Li, X. G.; Xu, X. G. High-resolution, full-color quantum dot light-emitting diode display fabricated via photolithography approach. *Nano Res.* **2020**, *13*, 2485–2491.

[15] Colvin, V. L.; Schlamp, M. C.; Alivisatos, A. P. Light-emitting diodes made from cadmium selenide nanocrystals and a semiconducting polymer. *Nature* **1994**, *370*, 354–357.

[16] Dai, X. L.; Zhang, Z. X.; Jin, Y. Z.; Niu, Y.; Cao, H. J.; Liang, X. Y.; Chen, L. W.; Wang, J. P.; Peng, X. G. Solution-processed, high-performance light-emitting diodes based on quantum dots. *Nature* **2014**, *515*, 96–99.

[17] Mashford, B. S.; Stevenson, M.; Popovic, Z.; Hamilton, C.; Zhou, Z. Q.; Breen, C.; Steckel, J.; Bulovic, V.; Bawendi, M.; Coe-Sullivan, S. et al. High-efficiency quantum-dot light-emitting devices with enhanced charge injection. *Nat. Photonics* **2013**, *7*, 407–412.

[18] Coe, S.; Woo, W. K.; Bawendi, M.; Bulović, V. Electroluminescence from single monolayers of nanocrystals in molecular organic devices. *Nature* **2002**, *420*, 800–803.

[19] Lim, J.; Park, M.; Bae, W. K.; Lee, D.; Lee, S.; Lee, C.; Char, K. Highly efficient cadmium-free quantum dot light-emitting diodes enabled by the direct formation of excitons within InP@ZnSeS quantum dots. *ACS Nano* **2013**, *7*, 9019–9026.

[20] Li, L.; Reiss, P. One-pot synthesis of highly luminescent InP/ZnS nanocrystals without precursor injection. *J. Am. Chem. Soc.* **2008**, *130*, 11588–11589.

[21] Xie, R. G.; Battaglia, D.; Peng, X. G. Colloidal InP nanocrystals as efficient emitters covering blue to near-infrared. *J. Am. Chem. Soc.* **2007**, *129*, 15432–15433.

[22] Li, D.; Kristal, B.; Wang, Y. J.; Feng, J. W.; Lu, Z. G.; Yu, G.; Chen, Z.; Li, Y. Z.; Li, X. G.; Xu, X. G. Enhanced efficiency of InP-based red quantum dot light-emitting diodes. *ACS Appl. Mater. Inter.* **2019**, *11*, 34067–34075.

[23] Li, Y.; Hou, X. Q.; Dai, X. L.; Yao, Z. L.; Lv, L. L.; Jin, Y. Z.; Peng, X. G. Stoichiometry-controlled InP-based quantum dots: Synthesis, photoluminescence, and electroluminescence. *J. Am. Chem. Soc.* **2019**, *141*, 6448–6452.

[24] Won, Y. H.; Cho, O.; Kim, T.; Chung, D. Y.; Kim, T.; Chung, H.; Jang, H.; Lee, J.; Kim, D.; Jang, E. Highly efficient and stable InP/ZnSe/ZnS quantum dot light-emitting diodes. *Nature* **2019**, *575*, 634–638.

[25] Cao, F.; Wang, S.; Wang, F. J.; Wu, Q. Q.; Zhao, D. W.; Yang, X. Y. A layer-by-layer growth strategy for large-size InP/ZnSe/ZnS core-shell quantum dots enabling high-efficiency light-emitting diodes. *Chem. Mater.* **2018**, *30*, 8002–8007.

[26] Lim, J.; Park, M.; Bae, W. K.; Lee, D.; Lee, S.; Lee, C.; Char, K. Highly efficient cadmium-free quantum dot light-emitting diodes enabled by the direct formation of excitons within InP@ZnSeS quantum dots. *ACS Nano* **2013**, *7*, 9019–9026.

[27] Zhang, H.; Hu, N.; Zeng, Z. P.; Lin, Q. L.; Zhang, F. J.; Tang, A. W.; Jia, Y.; Li, L. S.; Shen, H. B.; Teng, F. et al. High-efficiency green InP quantum dot-based electroluminescent device comprising thick-shell quantum dots. *Adv. Opt. Mater.* **2019**, *7*, 1801602.

[28] Moon, H.; Lee, W.; Kim, J.; Lee, D.; Cha, S.; Shin, S.; Chae, H. Composition-tailored ZnMgO nanoparticles for electron transport layers of highly efficient and bright InP-based quantum dot light emitting diodes. *Chem. Commun.* **2019**, *55*, 13299–13302.

[29] Li, Y.; Li, D.; Kristal, B.; Feng, J.; Lu, Z.; Chen, Z.; Li, X. Enhanced efficiency of InP-based red and green quantum dot light-emitting diodes. *SID Symp. Dig. Tech. Pap.* **2020**, *51*, 960–963.

[30] Lee, T.; Hahm, D.; Kim, K.; Bae, W. K.; Lee, C.; Kwak, J. Highly efficient and bright inverted top-emitting InP quantum dot light-emitting diodes introducing a hole-suppressing interlayer. *Small* **2019**, *15*, e1905162.

[31] Hofmann, S.; Thomschke, M.; Lüessem, B.; Leo, K. Top-emitting organic light-emitting diodes. *Opt. Express* **2011**, *19*, A1250–A1264.

[32] Wang, H. C.; Zhang, H.; Chen, H. Y.; Yeh, H. C.; Tseng, M. R.; Chung, R. J.; Chen, S.; Liu, R. S. Cadmium-free InP/ZnSeS/ZnS heterostructure-based quantum dot light-emitting diodes with a ZnMgO electron transport layer and a brightness of over 10,000 cd·m^{-2}. *Small* **2017**, *13*, 1603962.

[33] Ghosh, S.; Ghosh, M.; Kumar, P.; Sarkar, A. S.; Pal, S. K. Quenching of the excitonic emission of ZnO quantum dots due to Auger-assisted hole transfer to CdS quantum dots. *J. Phys. Chem. C* **2016**, *120*, 27717–27723.

[34] Shi, A. M.; Sun, J. H.; Zeng, Q. H.; Shao, C.; Sun, Z. C.; Li, H. B.; Kong, X. G.; Zhao, J. L. Photoluminescence quenching of CdTe/CdS core-shell quantum dots in aqueous solution by ZnO nanocrystals. *J. Lumin.* **2011**, *131*, 1536–1540.

[35] Zhang, Q.; Gu, X. B.; Zhang, Q. S.; Jiang, J.; Jin, X.; Li, F.; Chen, Z. P.; Zhao, F.; Li, Q. H. ZnMgO: ZnO composite films for fast electron transport and high charge balance in quantum dot light emitting diodes. *Opt. Mater. Express* **2018**, *8*, 909–918.

[36] Kim, H. M.; Cho, S.; Kim, J.; Shin, H.; Jang, J. Li and Mg Co-doped zinc oxide electron transporting layer for highly efficient quantum dot light-emitting diodes. *ACS Appl. Mater. Inter.* **2018**, *10*, 24028–24036.

[37] Liu, G. H.; Zhou, X.; Chen, S. M. Very bright and efficient microcavity top-emitting quantum dot light-emitting diodes with Ag electrodes. *ACS Appl. Mater. Inter.* **2016**, *8*, 16768–16775.